CERN-ACC-NOTE-2018-0041

5 September 2018
Arek.Gorzawski@cern.ch

Fast loss analysis with LHC diamond detectors in 2017

A. Gorzawski, S. Redaelli, N. Fuster–Martinez, H. Garcia–Morales, B. Salvachua, A. Mereghetti, C. Xu, G. Valentino, R. Appleby

Keywords: beam loss, collimator, halo, scraping, jaw, diagnostics, bunch by bunch, diamond loss detector, blm, 16L2

Summary

Four diamond detectors that provide beam loss measurements with time resolution in the nanosecond range were added in the vicinity of the primary collimators of the Large Hadron Collider (LHC). This is a powerful diagnostic tool that provides the unique chance to measure bunch–by–bunch losses. The operation of the LHC in 2017 presented several unusual events of fast, high–intensity beam losses, many of them captured by the diamond detectors in the betatron cleaning region. In this paper we review some of the relevant loss cases that were analyzed in the wider scope of determining the source of the instability generating these losses. We show a few possible applications of these detectors in daily operations.

Contents

1 Introduction

The possibility for measuring fast beam losses is important for present and future accelerators. In this note we discuss and present results from many experiments and measurements that we performed in 2017 with LHC beams mainly as a part of the standard operation. This note summarizes the observations and analysis concerning the data coming from the diamond beam loss monitors installed in the betatron cleaning region of the LHC, collected during the standard operation and during various machine development periods.

As a result of the nonconformity in cell 16L2, data from a set of beam dumps was recorded during the run. As they heavily affected the availability of the machine we used the diamond loss detectors to track down the beam behavior in a short lapse of time before the dumps occurred. We do not present the data analysis of these events in this note as other summarizing notes, e.g. [1] are covering this in detail. However, here we refer to the measurement configuration set up in the collimation region as well as in 16L2. In few places we refer as well to the functional limitations that we struggled working with all installations.

2 Layout and data acquisition system

2.1 Instrumentation layout

The diamond loss detectors (dBLM) are installed in various locations in the LHC tunnel [2] as showed in Fig. 1. Apart from the injection/ extraction quality checks and MD UFO test locations, the content and results presented in this note are related to losses recorded in the betatron cleaning region of the LHC (IR7). Two sets of measurement devices i.e. detectors and acquisition boxes, were set up in this cleaning region. For each beam, one downstream of the primary collimators (TCP) and a second one downstream of the secondary collimator where the special crystal collimators are located [3]. In both locations one diamond detector is installed for each beam, we annotate them later as dBLM-B1-1 for the TCP unit and dBLM-B1-2 for the crystal unit (Xtal), for the LHC Beam 2, names are respectively changed to dBLM-B2-1 and dBLM-B2-2.

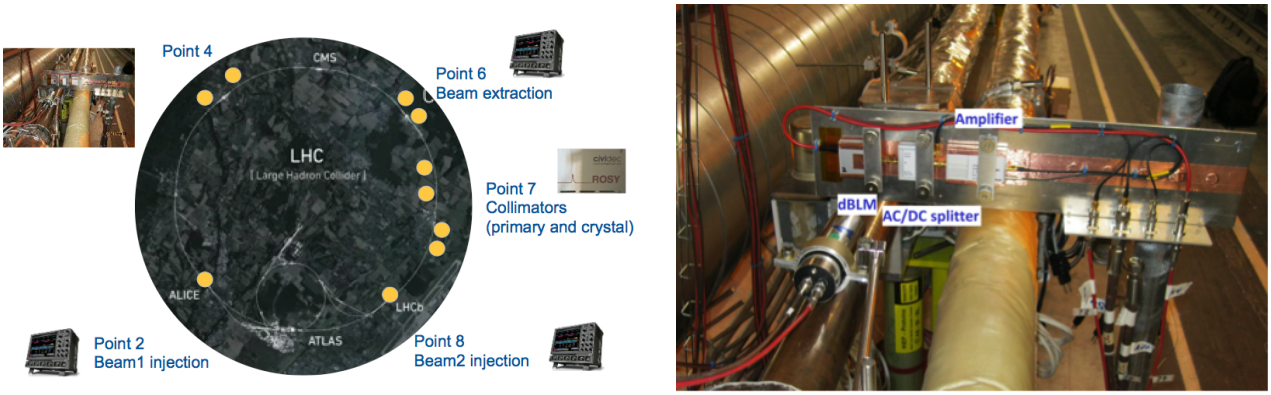

(a) (b)

Figure 1: The layout for diamond detectors installed in the LHC in 2017 (a) and the installation in the tunnel (b).

The detectors are polycrystalline diamonds with a size of 10 mm x 10 mm x 0.5 mm. Each detector is connected to an AC–DC splitter, where the AC-part of the signal is amplified by a current amplifier with a 20 dB gain and a bandwidth of 2 GHz. The whole detector system is provided by the *CIVIDEC*

instrumentation GmbH from Vienna, Austria. The detector system is mounted on a metal panel on top of the beam pipe (see Fig. 1b). The coaxial cable which connects the detector system to the read–out system is about 250 m meters long[1]. The diamond detectors are operated with a bias voltage of 500 V. Figure 2 shows the connection for the diamonds installed in TCP region. Table 1 lists the positions of each dBLM and their distances from the first TCP as $\Delta s_{TCP.D}$

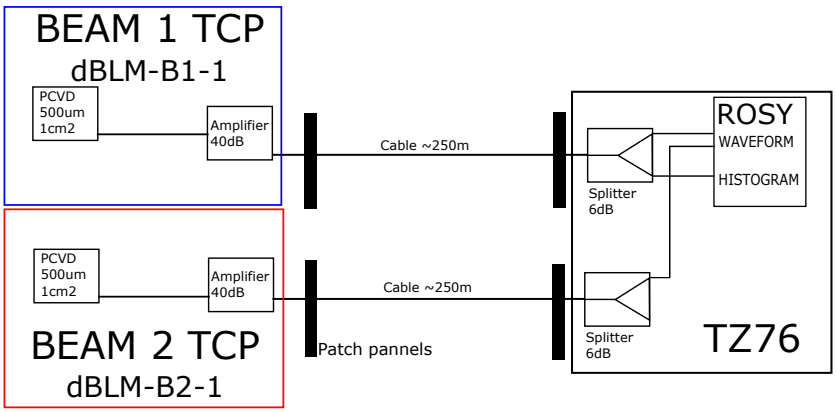

Figure 2: The TCP diamonds schematic connection including splitters and amplifiers along the signal cables.

Table 1: Absolute and relative positions for the diamond loss detectors installed in IR7.

parameter	TCP.D	dBLM TCP	dBLM Crystal
Beam 1		dBLM-B1-1	dBLM-B1-2
s [m]	19789	19800	19918
$\Delta s_{TCP.D}$ [m]	0	**11**	**129**
Beam 2		dBLM-B2-1	dBLM-B2-2
s [m]	20199	20189	20140
$\Delta s_{TCP.D}$ [m]	0	**10**	**59**

The detector signals in point 7 are read out by the ROSY data acquisition system also provided by CIVIDEC. The ROSY system comes with all the acquisition and triggering functionalities of a digital oscilloscope. In addition, an integrated FPGA provides dead–time–free online signal processing. The ROSY system has an embedded Linux operating system and provides a programmable interface to control the system and transfer the acquired data. This system is installed in the LHC service tunnel and is connected to the CERN technical network via an Ethernet cable.

2.2 ROSY read–out: histogram mode (HM)

In the histogram mode, the system is simultaneously able to produce a high sampling rate waveform and provide a real-time beam loss time histogram. The source signal is looped (by synchronization to the LHC turn time of ≈89 μs) and divided in time bins, with an individual counter set. The bin width is 1.6 ns. This mode is continuously recording at an update rate of 1 Hz. Figure 3 explains the operational principle of the histogram mode. The output of this read-out is a histogram with about 55700 bins

[1]This was the configuration for Beam 1 and Beam 2 near the TCPs. In mid 2017, when a similar installation was put in place in 16L2, the amplification and cable length had been adapted to the location requirements from ca.250 m to ca.500 m.

(mapping the LHC ring and bucket configuration). The corresponding bin is incremented when the signal recorded by the dBLM in that 1.6 ns region is larger than a pre-configured threshold.

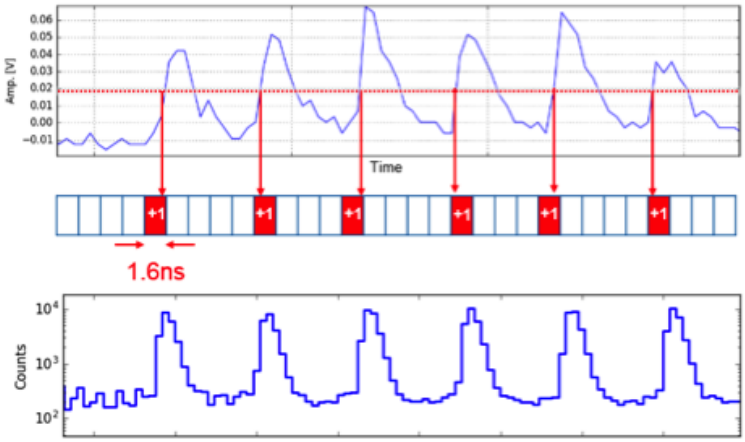

Figure 3: Beam loss signals exceeding a threshold (red line in the upper plot) causes the corresponding bin to increase in value.

2.3 ROSY read–out: waveform mode (WM)

In the waveform mode, the ROSY system has 4 analogue input channels for the waveform measurement. This is a direct oscilloscope–like measurement that records the signal with a defined sampling rate, length and voltage range. Each channel has a maximum sampling rate of 5 GS/s. A maximum buffer size of 10^9 samples is available to store the data from all 4 channels. Typically, 10^6–10^8 data points (i.e., ≈100 ms at the lowest sampling time of 1.6 ns) per channel were used, as any larger value significantly reduced the availability of the device.

2.4 Data acquisition and analysis code

A Python script has been developed to configure the ROSY system and store the detector data from both types of measurement for offline analysis. The script utilizes the PyJapc library [4], which is developed in the BE-BI group, to obtain LHC machine status parameters, starting and stopping the data acquisition automatically depending on the machine status. The measurement data are compressed and uploaded to the CERN EOS file system for long–term storage [5, 6]. An independent graphical user interface (GUI) has been developed to provide on–line monitoring and a quick review of the detector data without interrupting the data acquisition process. Both are accessible under [7].

A set of Python tools has been developed for simplifying the analysis of multi–turn bunch–by–bunch data. The tools are available under [8] and ready to use for the selected operations (consisting of data extraction and plot):

1. The integrated bunch by bunch loss along the bunch train within a given time window (HM)
2. The bunch–by–bunch loss time evolution (HM)
3. The bunch–by–bunch, turn by turn loss evolution (WM)
4. The bunch–by–bunch turn by turn frequency analysis, i.e. bunch tunes (WM)

2.5 Measurement limitations

2.5.1 Saturation and baseline drifts

During the operation with both cases, devices located at the vicinity of TCPs (high losses) and next to 16L2 (very small losses), we encountered few limitations related to the range of the recorded signal. These are general features that affect dBLM devices installed in all points not only in the vicinity of the primary collimators in Point 7.

If losses approach 7 Gy/s, which can be easily achieved in the standard cleaning mechanism from the primary collimators[2], the 2017 set–up (amplifier and attenuators) leads to saturation effects and eventually to non–physical signals recorded (see Fig. 4a). For the 2017 operation set–up, for the TCP saturation level in the acquired signal is set at 0.1 V, that corresponds (for the TCP configuration) to the 1 V signal at the amplifier input.

Related to the above, a constant operation with high losses introduces the baseline drifts (see Fig. 4b) called 'droop' [9]. Both, saturation and base line effect corrections are described in the next section.

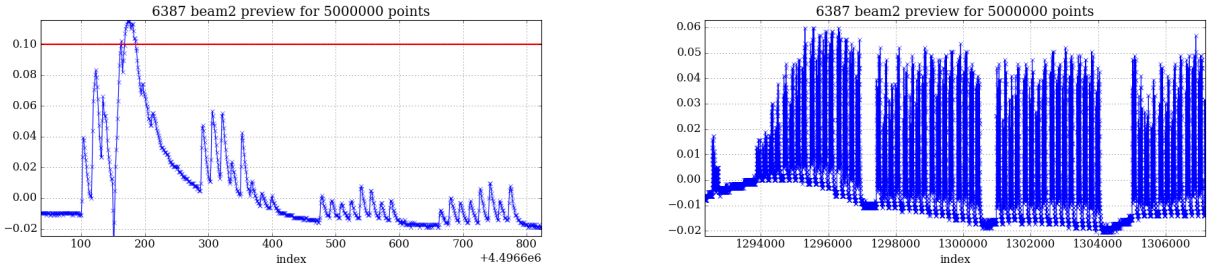

(a) Saturation **(b)** Baseline *droop*

Figure 4: Example of the base line *droop* (b) in one of the very intense loss (at the TCP) and saturation of the signal with too high loss (a) in the waveform mode. The red line indicates level 0.1 V that is the saturation effect of the amplifier.

2.5.2 Signal correction

In order to use the recorded signal in the waveform mode, we had to apply signal correction mechanism for the effects described above. The algorithm is based on the detection of the peak to peak height by finding the three consecutively rising values. After the base to peak value is found, it is saved as an absolute value for the peak. Figure 5 shows the result of the algorithm that was developed in order to have the usable data. Unfortunately, there is no mean to restore the saturated signal, see Fig. 5a where our approach simply removes non–physical values and then replaces by zero. However, a visible positive result for the *droop* (see Fig. 5b) was obtained and it was sufficient for the extreme cases, when too high loss occurred in the TCP region. This functionality will be introduced at the electronics level in the next generation system.

As show in the Fig. 5a, the information on the losses for the bunches immediately after the saturating peak values is lost. We consider it as lost anyway, as it was recorded in non operational regime at around 1 V here with corresponding 0.1 V, therefore we consider only the data samples with the raw value less than 0.1 V.

[2] This value was found empirically during various dump events by comparing the regular ionization chamber measurements and time evolution of the measured diamond signal.

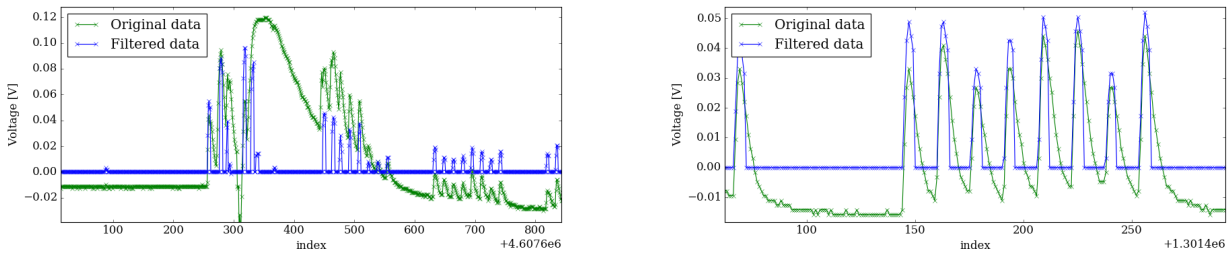

(a) Saturation **(b)** Baseline *droop*

Figure 5: Example of the saturation of the signal and its correction (a) and the significant baseline droop (b) in one of the very intense loss (TCP). Both cured with post processing correction algorithm.

2.5.3 Trigger method

While histogram mode can continuously be recorded for each LHC fill, the waveform mode requires triggering signal.

For the first part of the year the trigger was set as an absolute detected value threshold. With that setup a big fraction of the high beam losses occurring during regular operation were recorded, however in specific cases like Machine Developments a dedicated trigger was desirable. For the handling of trigger requests a timing card was requested and installed next to the ROSY box allowed setting up trigger on timing events. These two triggering method cannot coexist at the same time. Several relevant timing events were set to trigger the acquisition and only this triggering mode was used for the rest of the year. Section 3 summarizes the 2017 set–up including detailed information about the triggering process.

3 Machine configuration and diamond data scope in 2017

LHC configuration

In 2017, the LHC configuration changed a few times. For the purpose of this note, we decide to divide 2017 into three periods listed in Tab. 2. Two main changes occurred after the initial startup with nominal 25 ns trains of 48 bunches. First the filling scheme was changed as an immediate mitigation attempt for the vacuum nonconformity that raised the instability issues [1]. The change consisted of a switch from a standard 48 bunches train (48b) filling scheme to the trains (seven to eight in one batch) of eight bunches separated by four gaps (8b4e). Along this change, a smaller one concerning compression scheme was applied. The difference between standard and BCS [10] resulted in the reduced emittance. The second change was related to the optics, namely the β^* reduction from 40 cm to 30 cm after the second technical stop that occurred in September.

Table 2: Selected operation parameters for LHC in 2017 [11]. Half crossing angle was $\frac{\phi}{2}$=145 μrad and TCP half gap was kept at 5 σ during the collisions.

Period	Month	β^* [cm]	Beam Type
1	Apr – Aug	40	standard 25ns, 48b train
2	Aug – Sep	40	standard 25ns, 8b4e train
3	Sep – Dec	30	BCS 25ns, 8b4e train

Figure 6 shows the evolution of the total beam intensity stored in the machine along the year with some highlighted periods and events that happened during the year. The selected characteristic fill dumps are marked in the time line. Within the set of fills that lasted till physics production, fills with the strong electron cloud patterns, fills with 16L2 non–conformity activity, and isolated SQUEEZE/ADJUST single beam losses are showed. s

The "crossing–angle anti–levelling" [14, 15] is a luminosity levelling technique deployed at the LHC in 2017 that consists of reducing the angle in steps during the collision process, to increase the peak luminosity. Throughout the 2017 the LHC was operated following this method and the crossing angle changes were implemented in steps during the stable beams period, the period when experiments are taking collecting data.

Diamond data scope

In 2017, we essentially recorded all physics fills[3] with the TCP dBLMs and until September also with the crystal diamonds.

The HM recordings are available for all modes:

- for Beam 1 downstream TCP (dBLM-B1-1), and until September on downstream of crystal collimator (dBLM-B1-2),
- for Beam 2 downstream TCP (dBLM-B2-1) only from September till December.

The reason is the hardware restriction that only one histogram channel could be used per device, we reconfigured the system and we abandoned the crystal dBLM (dBLM-B1-2) and used the device with the TCP diamonds for the Beam 2 (dBLM-B2-1). With that change, as it showed later, no high–intensity signal (coming from the crystal sensor, here dBLM-B[12]-2) was recorded in the histogram mode and therefore some cycle analysis was not possible to do (see later in Sec. 4.1).

[3] A few fills were lost due to the interplay of configuration, supervision and communication errors or simple nonoperational system failures. Especially the hot, 16L2 periods in summer with detailed list in [12].

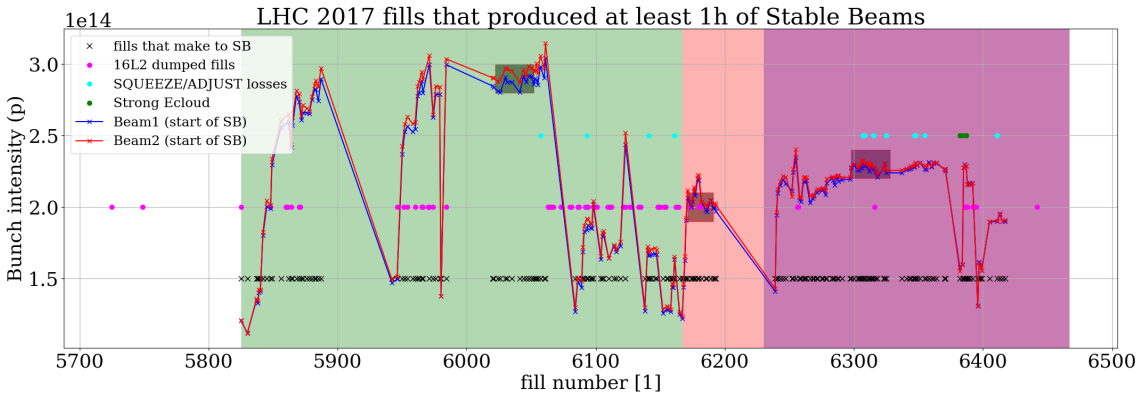

Figure 6: Evolution of the LHC total bunch intensity along the year (as a function of fill number). One can distinguish three main periods (see Tab. 2), operation with 48b scheme and β^*=40 cm (green), operation with 8b4e scheme and β^*=40 cm (red–ish) , and operation with 8b4e scheme and β^*=30 cm (magenta). Some other fills are marked with dots and crosses, e.g. fills with increased SQUEEZE/ADJUST losses or fills with a strong e-cloud pattern visible. Three shaded boxes represents group of fills that were considered in the later analysis.

The WM worked for Beam 1 (both sensors dBLM-B1-1/2) and Beam 2 (both sensors dBLM-B2-1/2). One has to keep in mind that these acquisitions were only triggered by beam dump events in standard operation. In addition, various test events were added to the system to trigger the acquisition during the dedicated tests i.e. collimator movements. Moreover, due to the large amount of data only modes with beam in were considered for the WM recording.

From th 9th of September we also measured and recorded also 16L2 events, with the same beam mode constraints as above. The summary if the operation setup for triggering of the waveform acquisition in 2017 mode is listed as follows:

- TCP ROSY Box (dBLM-B[12]-1)
  - Post Mortem event (Dump event)
  - Wire scanner on Beam 1 (for dedicated MD tests with Beam 1 only)
  - Collimator start timing
- Xtal ROSY Box (dBLM-B[12]-2)
  - Absolute threshold of 50 mV on Beam 1 OR Beam 2 (changed in a function of the MDs)
- 16L2 ROSY Box
  - Post Mortem event (Dump event)

Figure 7 indicates the periods of the year where different configurations of the existing diamonds and electronics were successfully operational.

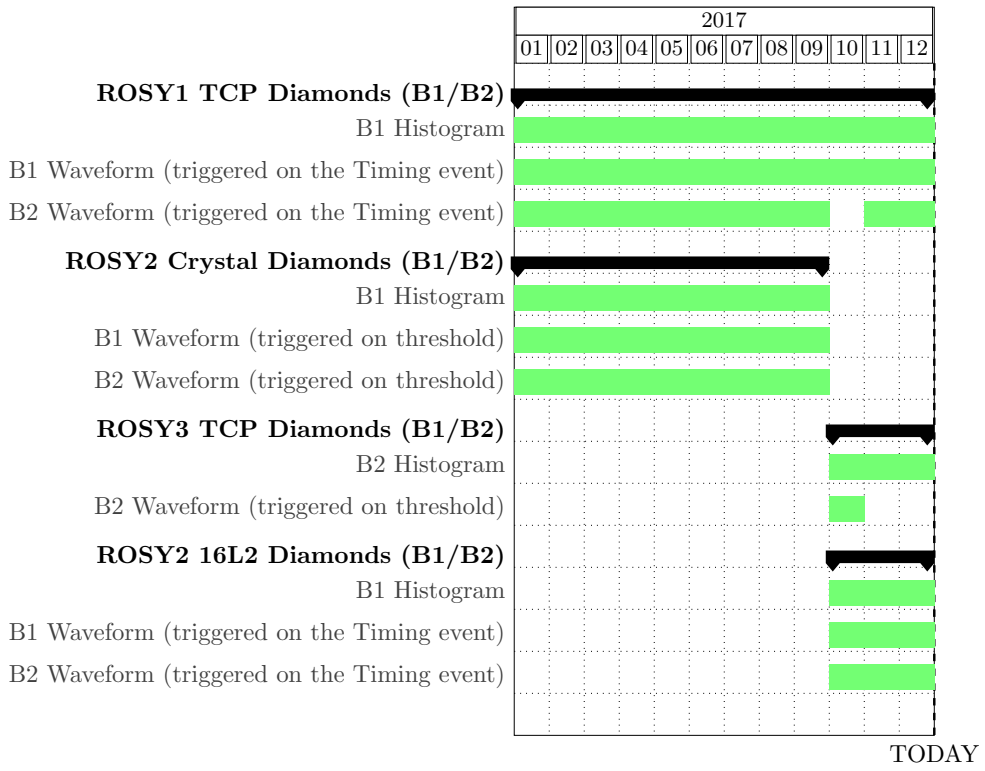

Figure 7: Three ROSY box configurations that were used used in 2017. ROSY3 before September was used for lab development.

4 Time loss histogram mode

As described in Sec. 2.2) one can monitor the HM with one second refresh rate, therefore longer ($\gtrapprox 10\,\mathrm{s}$) loss scenarios such as loss evolution over the given time period (i.e. LHC mode or time window) can show a big picture. As the bin resolution of this mode reaches 1.6 ns we see the separate bunch losses but we can not observe their losses in a quantitative way as it is impossible to get the magnitude of the loss. However, data recorded in this mode serves as a perfect input for the relative comparison in between the bunches.

4.1 Bunch–by–bunch loss evolution during OP cycle 2017

In this section we present a selection of results from the loss analysis of physics fills in 2017 in different phases of the LHC operational cycle. We consider only the standard physics production fills that produced at least one hour of Stable Beam (SB, see the shaded regions in Fig. 6) with total intensity larger than 2×10^{14}p per beam. In the middle of the year, due to instabilities coming from a vacuum nonconformity [1], the standard LHC filling scheme consisting of batches of 48 bunches spaced by 25 ns (48b) was replaced by a scheme featuring eight bunches separated by four empty 25 ns slots (8b4e). This gap limits effects from electron cloud. This scheme also benefited from smaller emittances, from $< \bar{\varepsilon} >$=2.5 μrad down to $< \bar{\varepsilon} >$=2.0 μrad, thanks to the batch compression scheme (BCS) [10]. Mean emittance used here is obtained from the subset of used fills and averaged over the respectively analyzed beam mode.

The selected fills represent three periods of the operational year: 48b operation, 8b4e scheme operation with β^*=40 cm and operation with 8b4e scheme with β^*=30 cm [4]. For these representative sets we focus on the following groups of bunch slots for each fill:

1. first non colliding train of 12 bunches,
2. colliding train at the beginning of the beam (later called *first colliding*),
3. colliding train at the end of the beam (later called *last colliding*),
4. the abort gap (AG) region in the filling scheme.

While a choice of 1/ and 4/ is rather obvious we selected 2/ and 3/ such as they match the same collision configuration and the number of long–range interactions.

Loss evolution per beam mode

Figures 8, 9 and 10 summarize the loss evolution for Beam 1[5]. We can see the average train loss in the representative trains over the three modes: RAMP, SQUEEZE and ADJUST, values are normalized to the losses recorded in the eight bunch train. Presented plots indicate that change of the filling scheme (see Tab. 2) decreased the bunch by bunch losses by an order of magnitude, this is possible due to the smaller beam emittance.

In general there is a stronger difference between colliding and non–colliding bunches visible for the 48b (blue) case than for the 8b4e (red) plots. Unfortunately, due to the configuration changes (see in Sec 3) made to the dBLM system no comparable data set can be found from the last period of the year (operation with 8b4e scheme and β^*=30 cm). Details about losses during that period can be found later in this section.

[4] Due to the configuration issues, swap of dBLM-B1-2 for dBLM-B2-1, for that period the data is extrapolated from the other detector, see Sec. 3 for configuration details.

[5] Beam 2 was only available in HM later in the year, see details in Sec 3

RAMP

Figure 8 shows the losses along the ramp. One can see the initial peak associated to the capture losses (see more detail later in the next subsection). The later peaks (as from around 600 s from the beginning of the ramp) come from the squeeze process that is partially incorporated in the ramp [13].

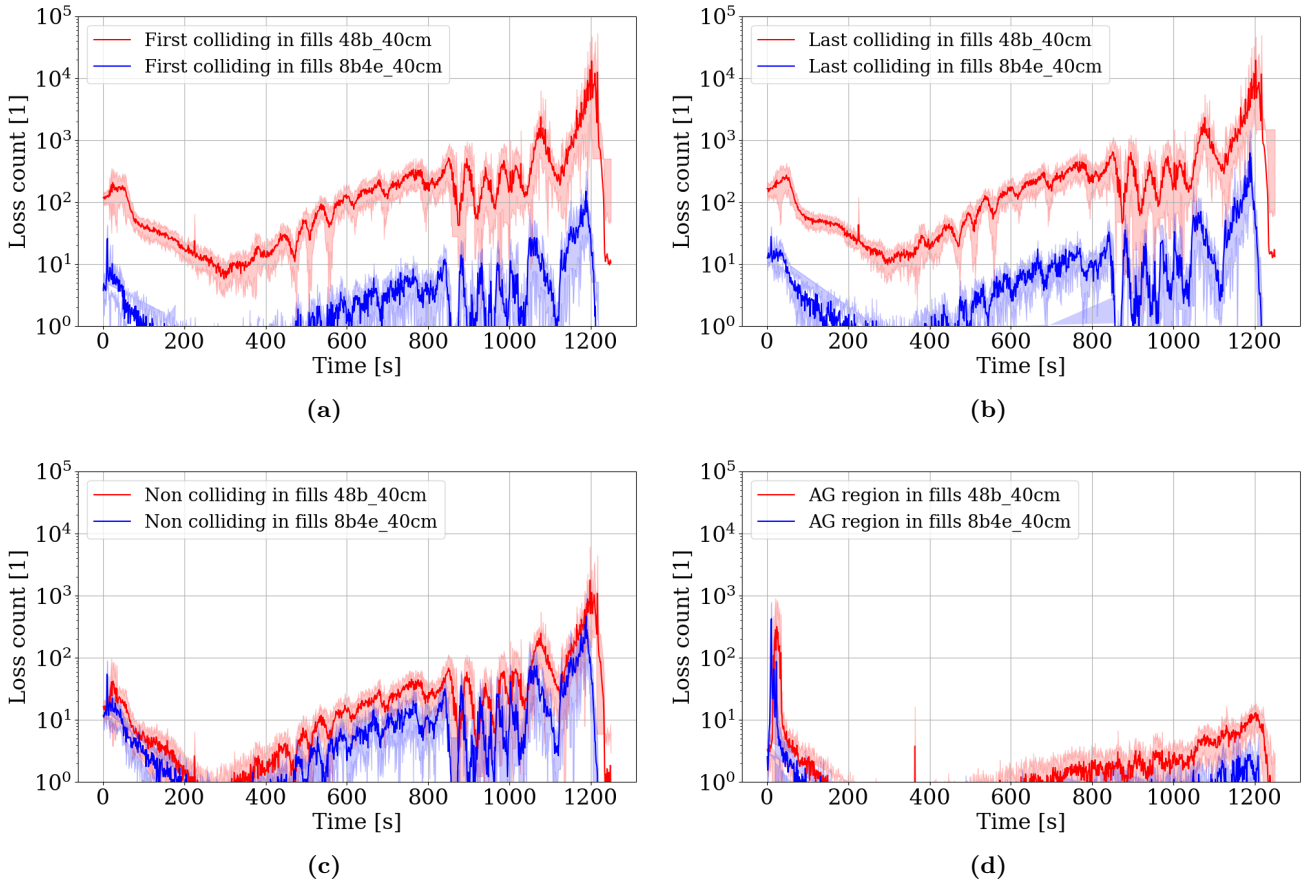

Figure 8: Histogram beam losses as a function of time during RAMP for Beam 1. Comparable losses can be seen for the non colliding bunches as well as for the AG region while the colliding trains represent an order of magnitude difference between those coming from the 8b4e scheme and 48b scheme.

SQUEEZE

Figure 9 shows the losses evolution over the squeeze process. One can see peaks associated to the points where the optics change occurs and when possible beta beat and orbit excursions are present.

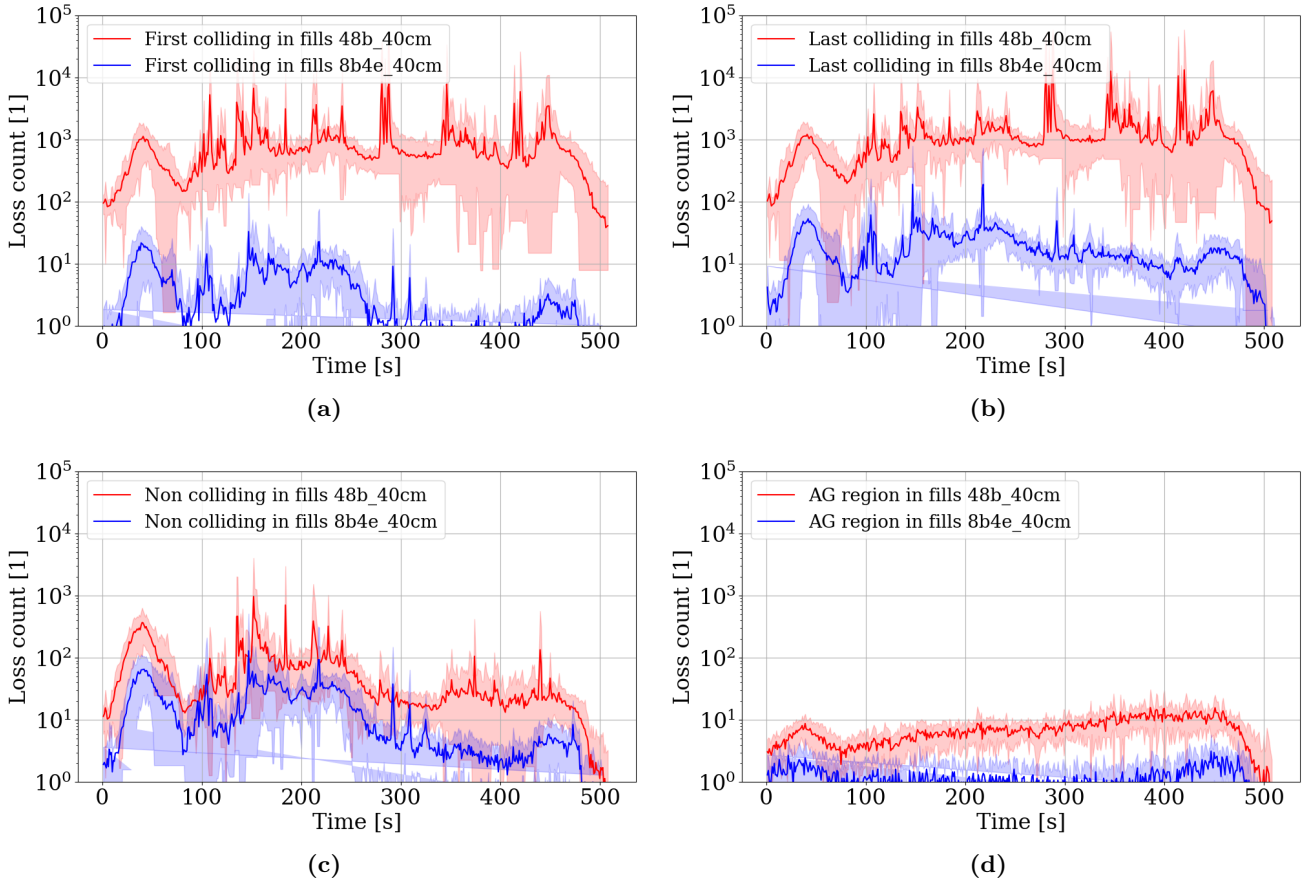

Figure 9: Histogram beam losses as a function of time during SQUEEZE for Beam 1. Less comparable than in the RAMP losses can be seen for the non colliding bunches as well as for the AG region while the colliding trains represent an order of magnitude difference between those coming from the 8b4e scheme and 48b scheme.

ADJUST

Figure 10 shows the losses evolution over the adjust process. In Figs. 10a and 10b one can see the loss peaks (at around 170 s from the beginning of adjust) that are associated to the collapse of the separation bumps (between 120 s and 220 s) in two IPs. The large spread visible around that moment is associated to the fact that the collapse was not always done in the same moment, as it is driven manually. Figure 10c shows the loss of the non colliding bunches before the collapse of the bumps is applied. As there is no dedicated step in the sequence that could affect directly the non colliding bunches, this spike could be attributed to some single bunch instability evolving at that time, examples can be found in Sec. 4.3.

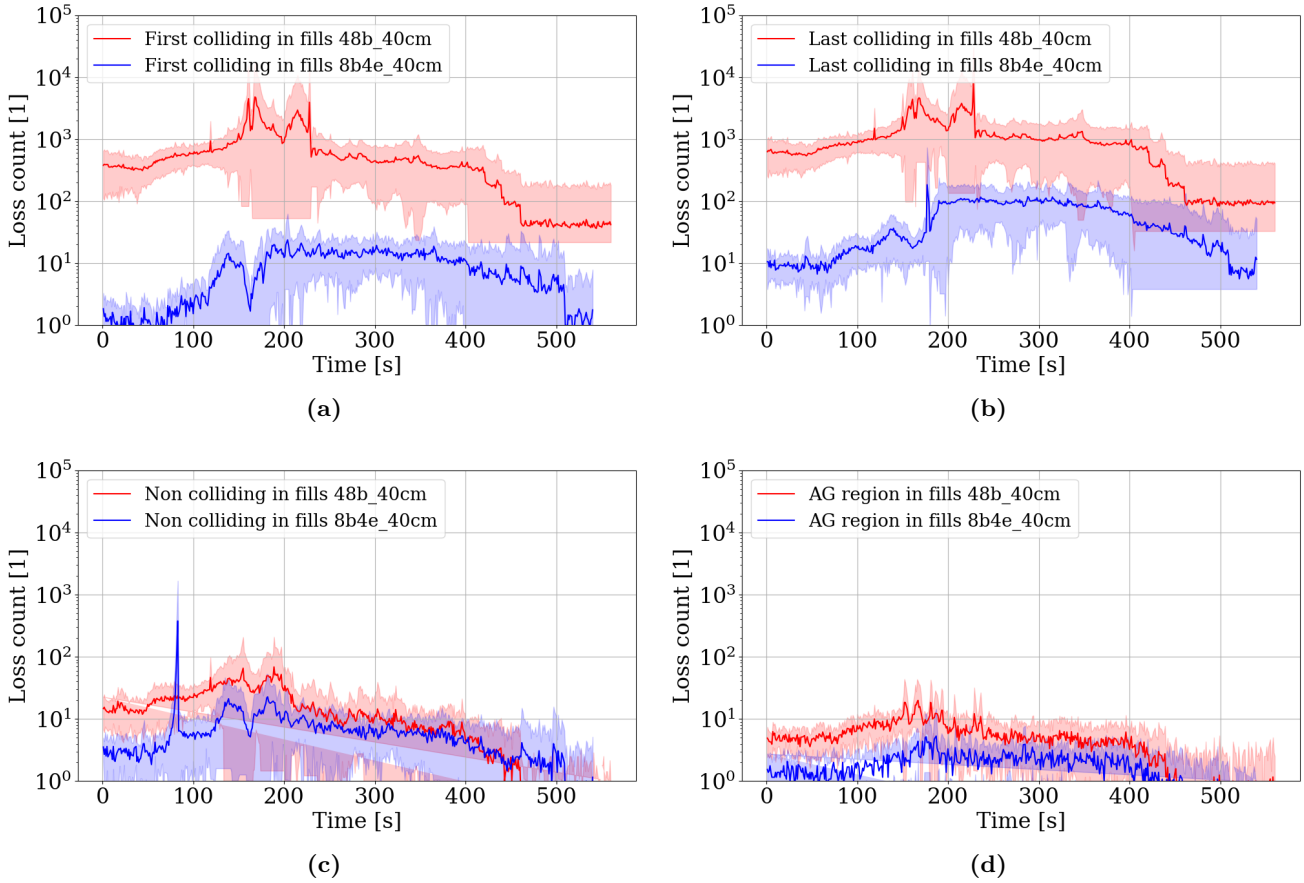

Figure 10: Histogram beam losses as a function of time during ADJUST for Beam 1. Less comparable than in the RAMP, losses can be seen for the non colliding bunches as well as for the AG region while the colliding trains represent an order of magnitude difference between those coming from the 8b4e scheme and 48b scheme.

Capture losses at the start of the ramp

As the RAMP mode begins, all the particles outside of the RF buckets are lost as the momentum of the beam is changing. They can be quantified by looking at losses seen in the AG when no filled RF buckets are present. Figure 11 shows the zoom of the capture losses at the beginning of the ramp from the populated AG.

While the absolute height of the loss peaks do not differ for both cases (before and after the filling scheme change) a puzzling time distribution can be noticed. For the reasons described in [17] that discuss the difference between the signal start of the ramp and the actual start, we plot the losses as from the time when SIS-RAMP-START timing event is published. However, despite including that correction for the time evolution, still a large spread in timing of the losses is visible for cases when operating with 48b scheme (red curves in Fig. 11) while is only a little spread for the 8b4e case.

As there was no fundamental change in the Ramp functions while changing the filling scheme, the origin of that effect is still not understood and needs more detailed analysis.

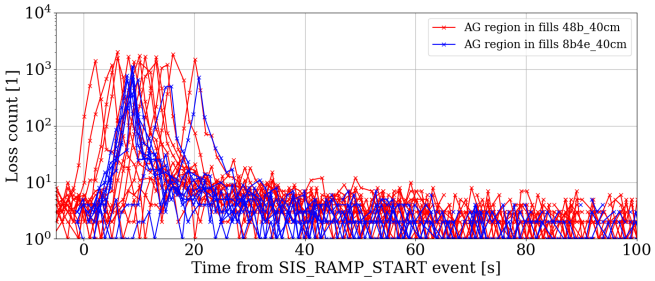

Figure 11: Beam 1 losses at the start of the ramp. One line represents one fill data, loss evolutions are shown for operation with 48b scheme and β^*=40 cm (red) and operation with 8b4e scheme and β^*=40 cm (blue). Time is aligned with the timing event sent to the power converters and collimators.

Losses in the cycle for β^*=30 cm

Due to the setup changes (see Sec. 3) over the year we found no direct way to compare the operation with β^*=40 cm and β^*=30 cm from the recorded loss point of view.

The averaged values for a given bunch groups coming from a set of fills in the corresponding periods of time (see fills in Fig. 6) is showed in Fig. 12. One can observe an increased value of the signal (base line) recorded in the β^*=30 cm period (see 12c). The *Last colliding* train trend indicates as well an increased level of losses that was often observed (for the trailing part of the beam) in this period and is shown in some more detail in Sec. 4.3.

Figure 13 shows the averaged subset of 8b4e β^*=30 cm fills for Beam 2 (dBLM-B2-1) with no indication of significant losses along the squeeze. For both cases, although the 30 cm SQUEEZE is longer than 40 cm, we plot only the corresponding and therefore comparable part.

During this analysis we observed that recorded signal level for Beam 1 and Beam 2 differed more than only difference in diamond characteristics and measurement configuration. A strong attenuation for the Beam 1 HM was visible. For the WM channel, this attenuation resulted in the lower signal during high loss scenarios while for the normal operation was not noticeable. As a result part of the Beam 1 set-up is expected to be replaced during the 2017/2018 winter stop.

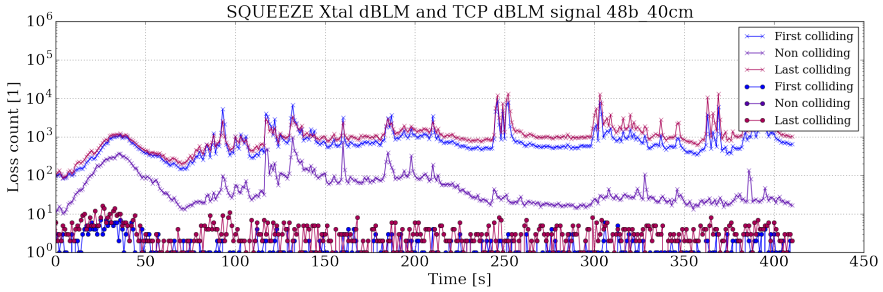

(a) 48b scheme and β^*=40cm

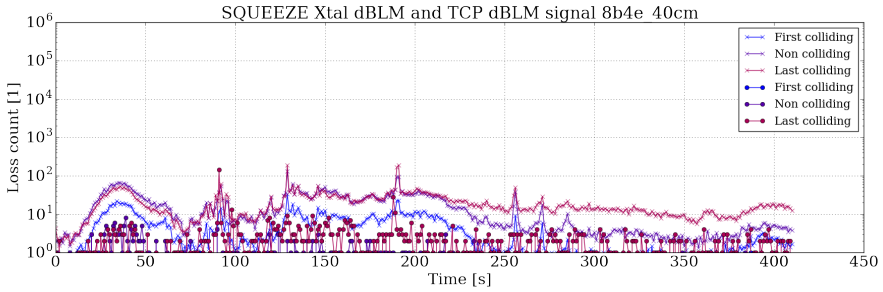

(b) 8b4e and β^*=40cm

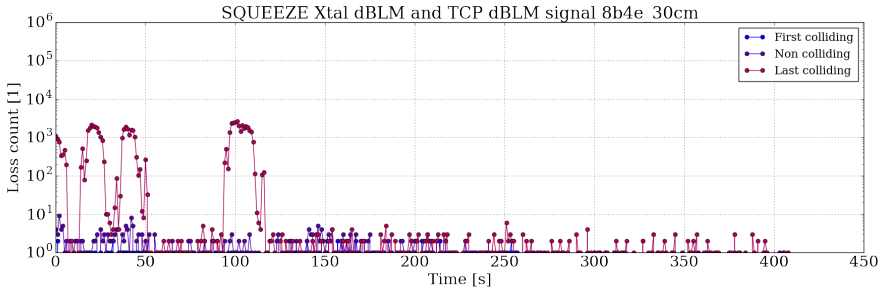

(c) 8b4e and β^*=30cm

Figure 12: Beam 1 loss during SQUEEZE recorded by diamonds on crystal location (lines, dBLM-B1-2) and directly on TCPs (dots, dBLM-B1-1). Each line represents an averaged evolution for one train family. There is a visible increase in loss when operating with β^*=30 cm indicated by signal recorded with dBLM-B1-1 diamonds.

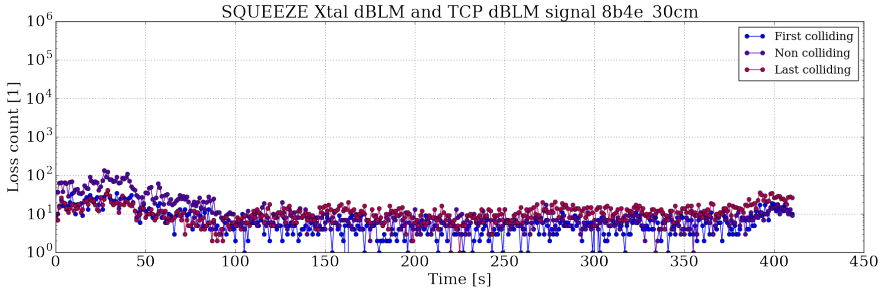

Figure 13: Beam 2 loss during SQUEEZE mode recorded in the last period with no increased losses visible. Signal recorded with dBLM-B2-1 diamonds during the 8b4e and β^*=30 cm period, after the changes described in Sec.3.

4.2 Bunch–by–bunch losses during the reduction of the crossing angle

Figure 14 shows the evolution of the losses of the different trains for 30 min before and after the first crossing angle change from 145 μrad to 140 μrad, usually around one hour after the declaration of the Stable Beam mode. Whereas the overall losses are visibly lower, an improved beam lifetime was seen

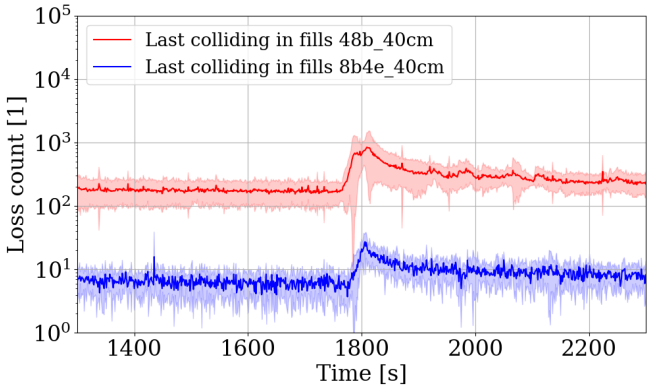

Figure 14: A loss evolution of the last colliding trains for two filling schemes (red for 48b and blue for 8b4e, both at the β^*=40 cm) during the crossing angle change. The spread represents the variation between the fills in the subset, see Tab. 2.

with a changed filling scheme 48b to 8b4e trains[6]. This might be attributed to the different long–range beam–beam pattern across the whole batch and therefore, different scraping effect when lowering the crossing angle.

Figure 15 shows loss evolutions for one type of trains in the beam for one representative fill for 48b [7] for three consecutive crossing angle changes from 145 μrad to 135 μrad in steps of 5 μrad. After each of those steps a luminosity optimization is performed in order to confirm the best orbit for luminosity production. Losses generated by this are illustrated at around two minutes after the actual step in crossing angle is done [16].

Figure 16 shows the overall profile of the integrated loss along the trains at the front and at the end of the beam for two cases 48b and 8b4e schemes. Those profiles quantitatively follow the pattern of long–range beam–beam encounters with higher losses in the center of the batch than at the head and tail. Although the overall losses for the 8b4e remains lower, a quantitatively similar pattern can be noticed in the 8b4e batches.

[6]For the reasons described in Sec. 3 we do not have data to picture this, but the general observations (BLMs, FBCTs etc. support that.

[7]Normal fill, with no abnormally short Stable beams period.

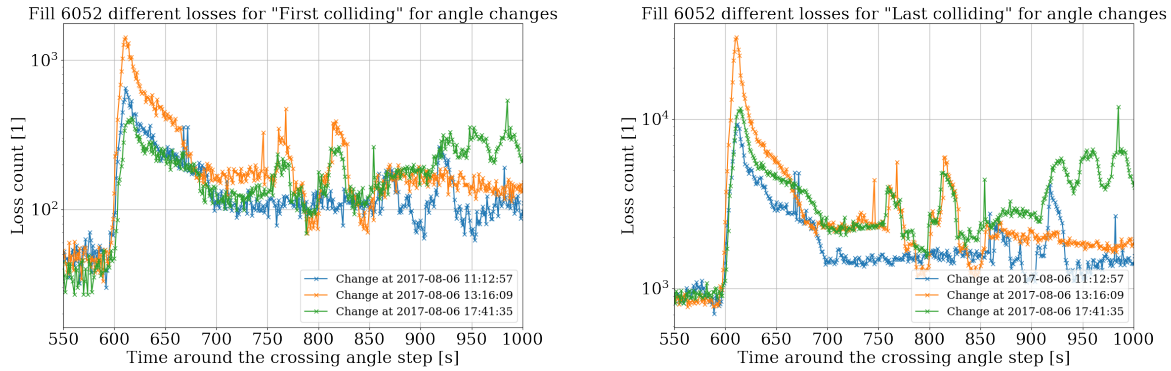

(a) first colliding train **(b)** last colliding train

Figure 15: An integrated loss evolution of colliding trains during the crossing angle changes applied during the Stable Beams loss recorded using dBLM-B1-2 detector.

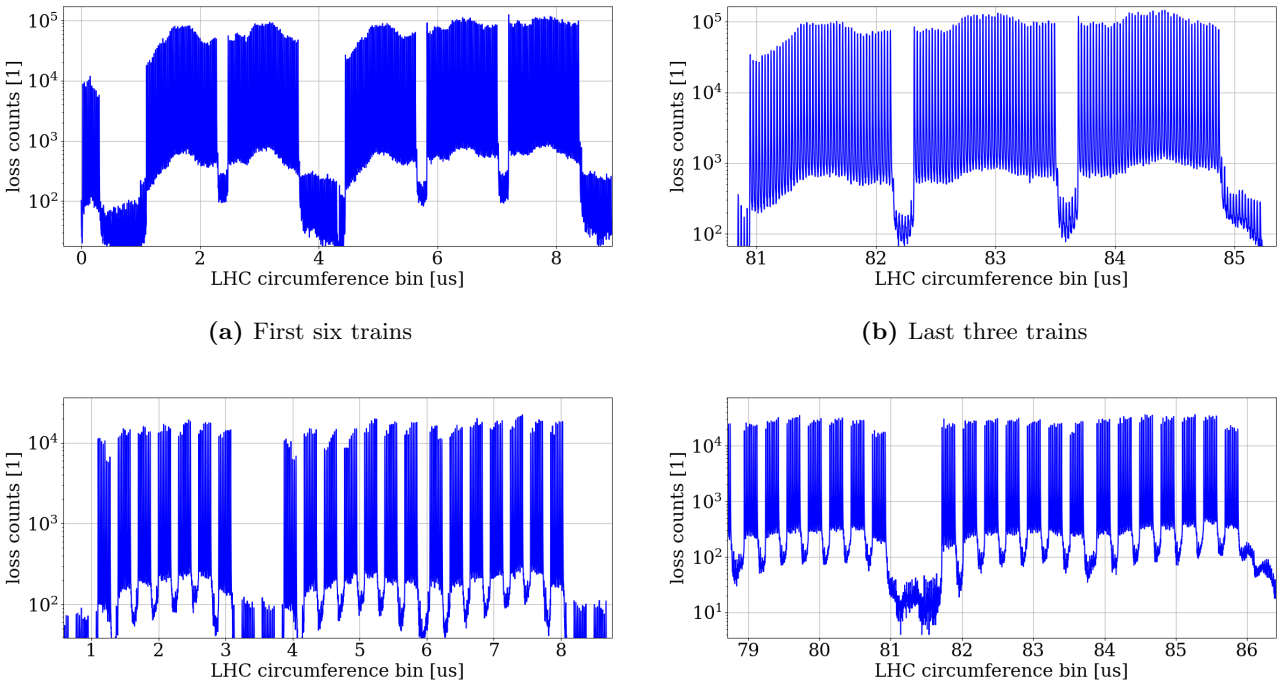

(a) First six trains **(b)** Last three trains

(c) First three batches of 8b4e trains **(d)** Last three batches of 8b4e trains

Figure 16: Selected representative loss profiles recorded during Stable Beams (for fills in 1/ and 2/ periods, see Tab.2).

4.3 Individual bunch losses in case of beam instabilities

The bunch–by–bunch resolution allows us to determine which bunches are responsible for losses in case of instabilities. We had introduced off–line monitoring scripts for bunch–by–bunch loss evolution during the cycle in order to identify the most active bunches. Figure 17 shows a loss evolution of the different bunch trains along the time in the given cycle with the aim of establishing correlations to the other observations, e.g. of transverse instability. Figures 17a and 17b shows the integrate loss count of all the bunches over given mode, here SQUEEZE and ADJUST. Isolated bunch slots with loss counts larger than 10^2 (arbitrarily chosen value) are plotted in Figs. 17c and 17d, where we can see their time evolutions with the moments when they started and ended.

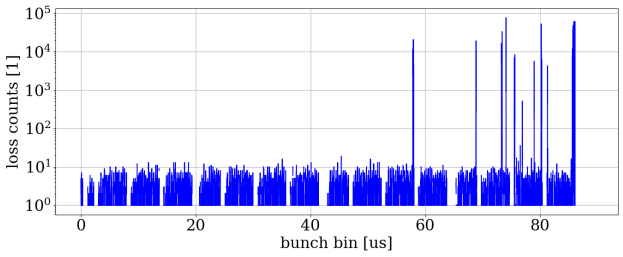

(a) integrated loss per bunch slot profile

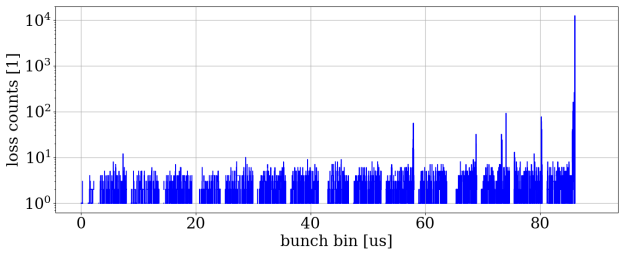

(b) integrated loss per bunch slot profile

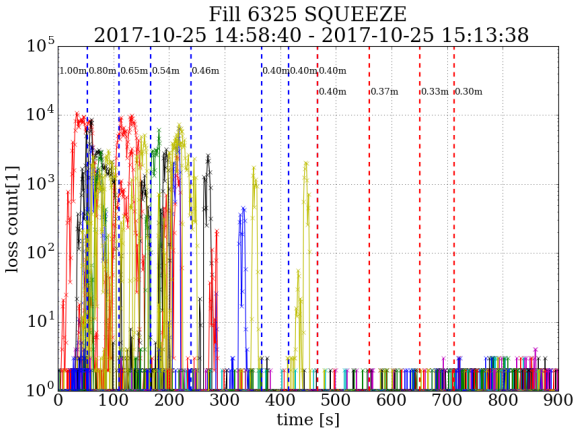

(c)

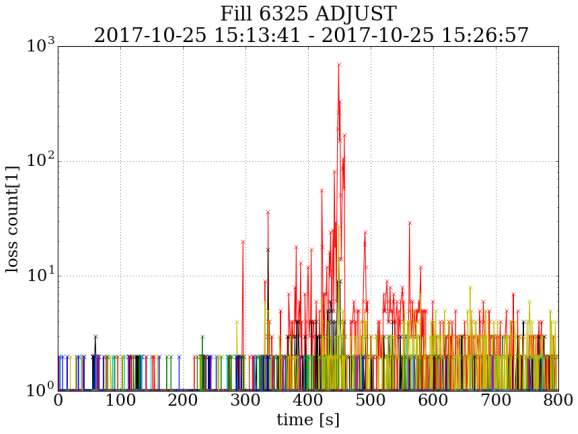

(d)

Figure 17: Illustration of the bunch trains loss evolution in SQUEEZE and ADJUST. Top row shows the profiles and indicates some bunch slots that loses more (spikes larger than 10^2). Bottom row, shows the time evolution of the active bunches with the indication of the activity time wrt to the start of the respective mode. Example illustrated thanks to the dBLM-B1-2 data.

4.4 Bunch–by–bunch diffusion measurements

In 2017 a long beam halo scraping campaign was performed. During these tests that were performed as an End–Of–Fill test, we moved one jaw (for both horizontal and vertical planes) of the collimator into the beam in small steps, resulting into the loss spikes. Analysis of those gives much information about the beam and particles in it. While the details of the experiments can be found in the separate notes [18, 19] the preview of the results are shown in the Fig. 18, where the bunch by bunch loss evolutions

during the scraping step are shown. A distinction for the colliding and non colliding bunches is shown as well as results of the fits.

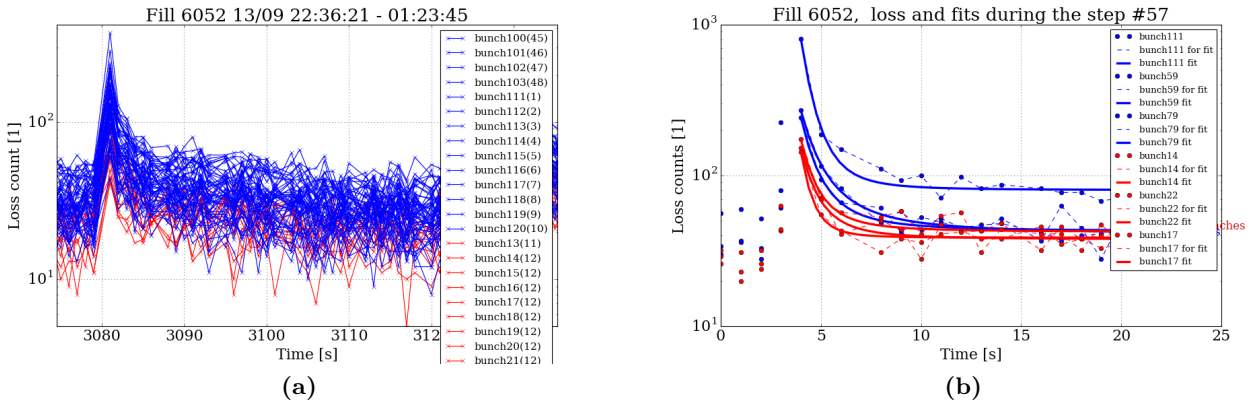

(a) **(b)**

Figure 18: Loss evolution over one collimator step during the beam scraping experiment [19] illustrated for selected bunches and colored as a function of colliding (blue) and non colliding (red) bunches (left). In the right, selected bunches with their evolution and fits done for finding of the diffusion parameter. Example illustrated thanks to the dBLM-B1-2 data.

4.5 A look at 2016 dBLM data

Most of the scripts and functions for analysis of these data were developed in 2017 but could be used for the analysis of data collected in 2016. We present few of the main applications of the same tool for data recorded still in 2016. Table 3 briefly recalls the main LHC operation parameters.

Table 3: Selected operation parameters for LHC in 2016 [11]. TCP half gap was kept at $5\,\sigma$ during the collisions.

Month	β^* [cm]	$\frac{\phi}{2}$ [μrad]	Beam Type
Apr – Sep	40	185	standard 25ns, 48b train
Sep – Nov		140	

Adjust instabilities

LHC run in 2016 was affected by some issues with single bunches becoming unstable during the ADJUST beam mode [20]. As the bunch–by–bunch beam intensity measurement was not fast enough to catch this changes, we looked at bunch–by–bunch losses.

In Fig. 19, we show two steps of the investigation needed for chasing of the increased losses. Figure 19a shows the peak detection algorithm, that looks for the higher loss leaks that identifies the interesting bunches. Figure. 19b shows the loss evolution in time. Illustrated here case, was a first try on the unstable bunch detection in 2016 that later evolved in the procedure already described earlier in Sec. 4.3

2016 crossing angle reduction

At the end of the 2016 proton Run, the LHC beams were collided at a reduced crossing angle. The implemented reduction was from 185 μrad to 140 μrad [21]. The first fill after the implementation was

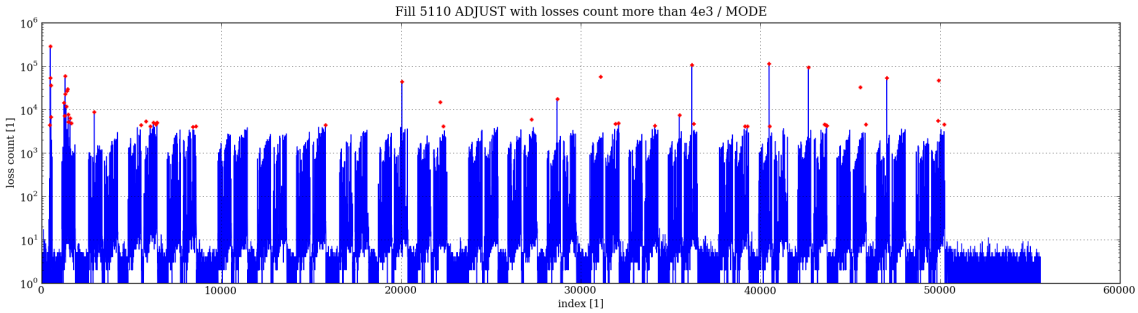

(a)

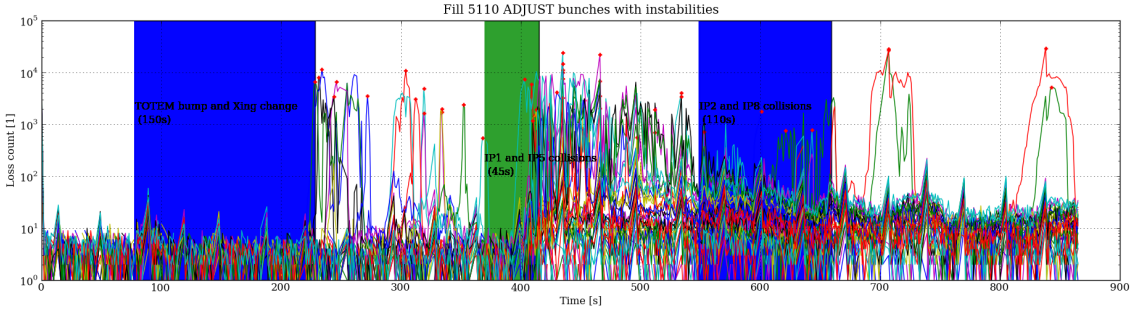

(b)

Figure 19: The overview of the most loosing bunches (marked with red dots) along the beam process (a) and the bunch by bunch evolution illustrating the time of instability arise (b).

done indicated a strong reduction of the beam lifetime. Again the bunch–by–bunch resolution of diamond detectors allowed comparing losses before and after that change, and identify the loss difference between the bunch families. The cause of those losses was traced to a non optimal tune working point [21]. Figure 20 shows three moments of that reduction, seen as losses for the non colliding and colliding bunches. The first shows the fill of the regular operation before crossing reduction, first fill with a reduced crossing angle and the following fill where the tune corrections found were included.

Figure 21 shows in detail the level of losses along the bunch train before and after applying the corrections were introduced plus the relation to the 'stable' moment in the cycle where no effect of the crossing angle is visible.

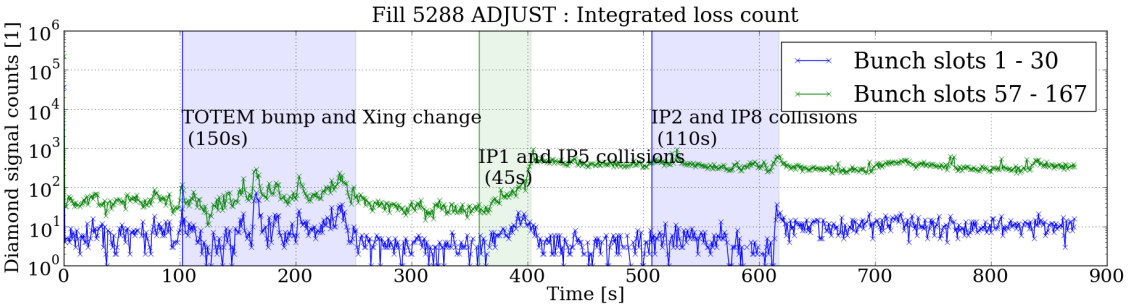

(a)

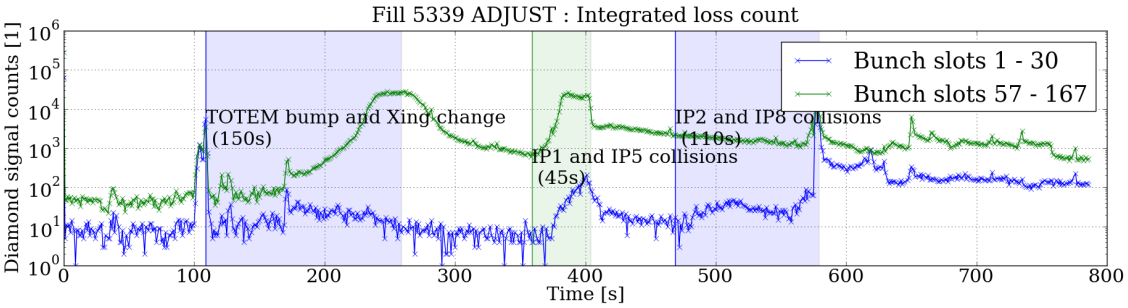

(b)

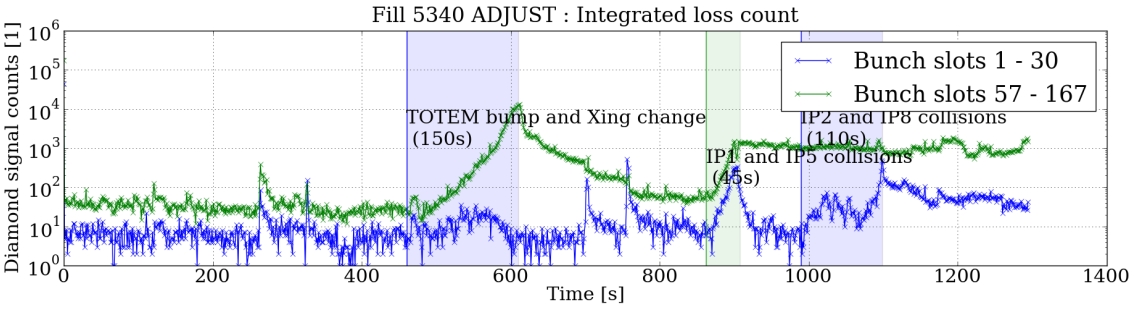

(c)

Figure 20: Illustration of the loss difference along the batch structure for before and after tune adjustment needed after the crossing angle reduction. Non colliding 12 bunches (slots 1-30) and two colliding trains (2x48b slots 57–167).

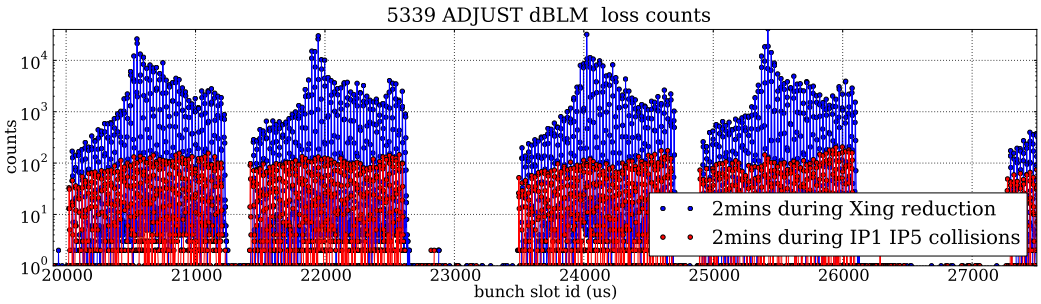

(a)

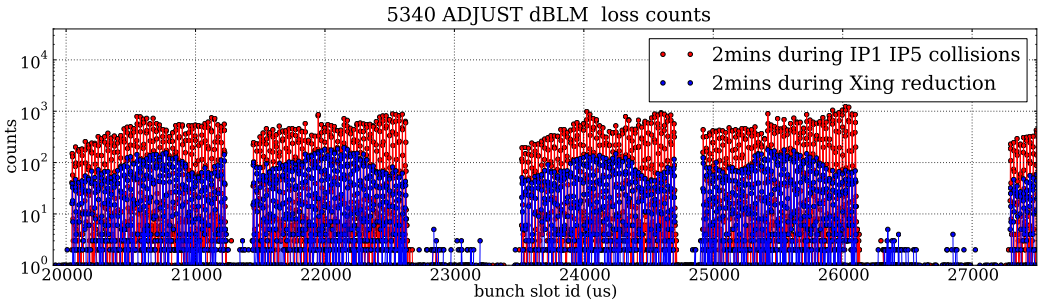

(b)

Figure 21: Losses integrated over two minutes after the collapse of the separation bump as a function of bunch slot for fill before 5339 and after 5340 tune adjustment needed after the crossing angle reduction. Blue plot noticeably indicates a reduction of the loss contribution during the crossing angle change.

5 Waveform mode

In the waveform mode (Sec. 2.3), one can specify the sampling frequency and the number of points that will be recorded. The larger part of data collected in 2017 run was recorded with 100 M samples, at 1.6 ns. As the system was still in development phase, few periods were ran at experimental settings i.e. varying the number of sampled points, sampling frequency etc. Due to these tests we have lost some data recorded during the physics fills.

5.1 Turn–by–turn and bunch–by–bunch losses

In order to extract the turn–by–turn and bunch by bunch information one needs to divide the initial signal of typically 100M samples spaced by 1.6 s into single–turn data, where turn is $\approx 89\,\mu s$. This is done thanks to the marker called turn clock (TurnClk) that is recorded as a separate channel in the data structure. Having this marker, a slicing of the signal can be done.

For the purpose of this analysis we use the external source for the filling pattern, coming from the Fast Beam Current Transformer (FBCT)[8] signal. Information for the expected bunch locations combined with the start times of each turn is then overlay with the loss pattern and the peak values for each bunch is extracted per turn. Figure 22 shows the bunch–finding procedure.

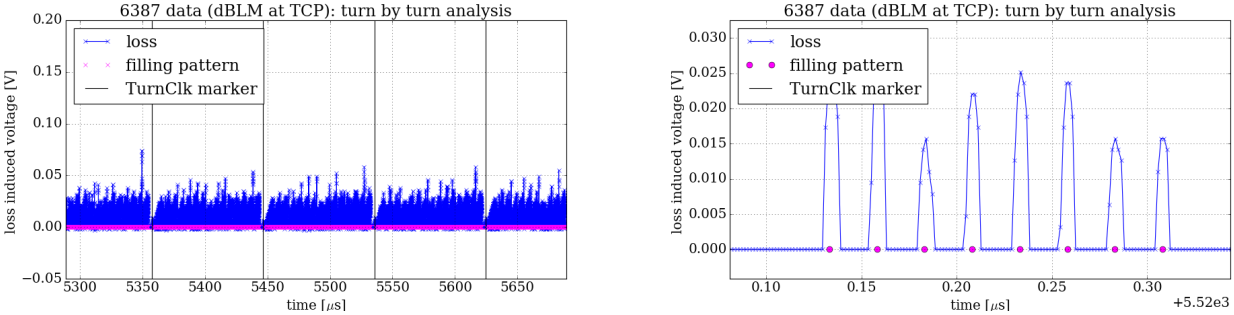

Figure 22: Illustration of the bunch pattern fit using the loss waveform, the turn clock markings and the FBCT filled bunches informations. In the left–hand side, four following turns with visible turn markers and aligned bunch slots (magenta). In the right–hand side a zoom for the eight bunches train with properly timed slots.

With our method, we agree to lose partial information about the total integrated loss voltage, namely the total lost charge in that case. To overcome that part we need better hardware correction for the future system (foreseen for the VFC installation) that can cope with the high dynamic range of the losses and limitations described in Sec. 2.5.

After aligning two time series of expected bunch slot positions and the actual loss we provide two ways of extracting the bunch loss information. The *default* is just the peak value of the bunch slot. The second consists in integrating for the bunch slot (Fig. 23) for a given number of samples. The later is only meaningful and correct for a raw signal that did not need the correction. As already shown and explained the correction reduces the physical meaning of the loss information (see this beginning of this section and Sec. 2.5).

The corrections and fine tuning showed in Sec. 2.5, allowed to reconstruct the turn–by–turn and bunch–by–bunch evolutions, especially useful for fast losses. We present some of the fast and high losses

[8] system that provides bunch–by–bunch beam population measurement.

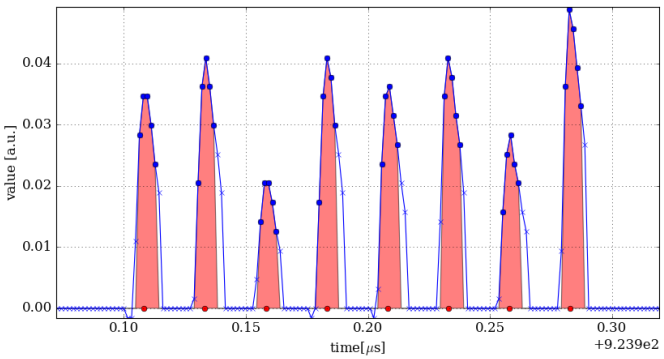

Figure 23: Illustration of integration around interpolated values. In blue the corrected loss signal, red points illustrate the expected bunch position and the red area illustrates the integration area.

cases (e.g. 16L2 case [1]). Figures 24 and 25 show multi turn loss evolution along the beam filling scheme. This break down of the bunch/turn contribution allows to identify the first unstable bunch for along the recorded turns. It allows as well to see the evolution of the profile loss, i.e. if a specific loss build up is identifiable along the batches.

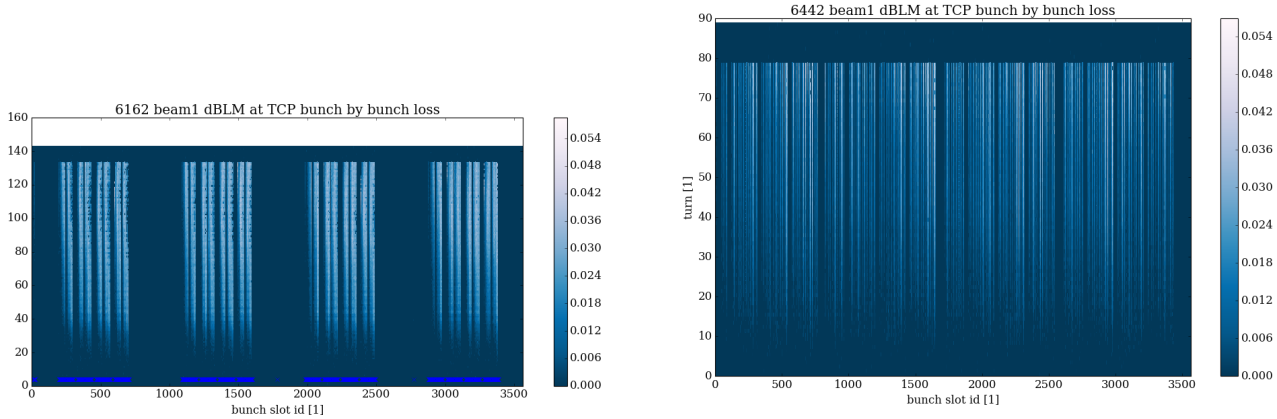

(a) **(b)**

Figure 24: Example of turn–by–turn and bunch–by–bunch reconstruction of the loss data recorded with the waveform mode For Beam 1.

5.2 Frequency analysis – Tune reconstruction

During the LHC 2017 run, various end of fill tests were performed that consisted scraping of the beams with primary collimators [19]. Based on this scans and some cases of long lasting (> few tens of turns) losses recorded in operation we present another usage of the diamond loss detectors – namely bunch by bunch tune reconstruction.

Provided that data is not heavily affected (see Sec. 2.5 and not much of the fixing algorithm needs to be run), after splitting into the turn–by–turn data we can perform its frequency analysis for given bunch slot evolution. Figure 26 shows two groups of bunches, that produce losses over the recording

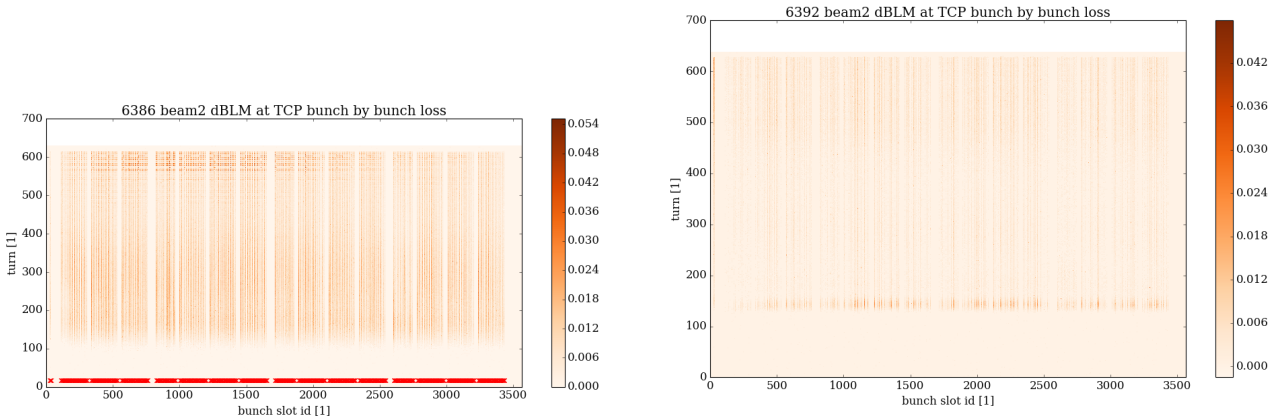

(a) **(b)**

Figure 25: Example of turn–by–turn and bunch–by–bunch reconstruction of the loss data recorded with the waveform mode for Beam 2.

time. Out of this data a selected bunch is treated separately for the tune measurements. First, the Hann window [22] is applied to improve the FFT algorithm (see Fig. 27). Later the FFT is performed on that signal and shown in Fig. 28. The final bunch spectrum is obtained by re–normalization to the equivalent sampling frequency (11245 Hz) and showed in Fig. 29. Figures 31 and 30 show the same procedure for a dedicated bunch that was recorded with higher losses during the collimator scraping experiments. For both cases there are many distinctive peaks obtained by the analysis. Two of them are close to the nominal betatron tunes.

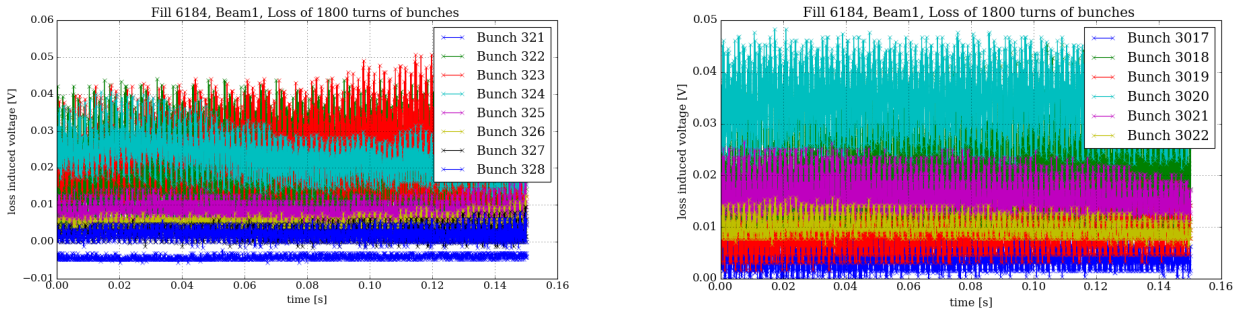

(a) **(b)**

Figure 26: Time evolution of selected bunches during the long lasting loss recorded just before the beam dump in fill 6184. Difference in loss levels is visible, but the frequency components are visible in all cases.

However, in order to use this for the bunch tune measurements it is obvious that dedicated losses are needed. Moreover, in order to provide a reliable result, one needs to foresee on the hardware side a reliable configuration for the amplifier (see Sec. 2.1). Moreover, due to the only overall loss information (combined Vertical and Horizontal) it is hard to disentangle Q_x and Q_y. It was proposed and accepted to install an additional detector to measure only vertical losses in 2018.

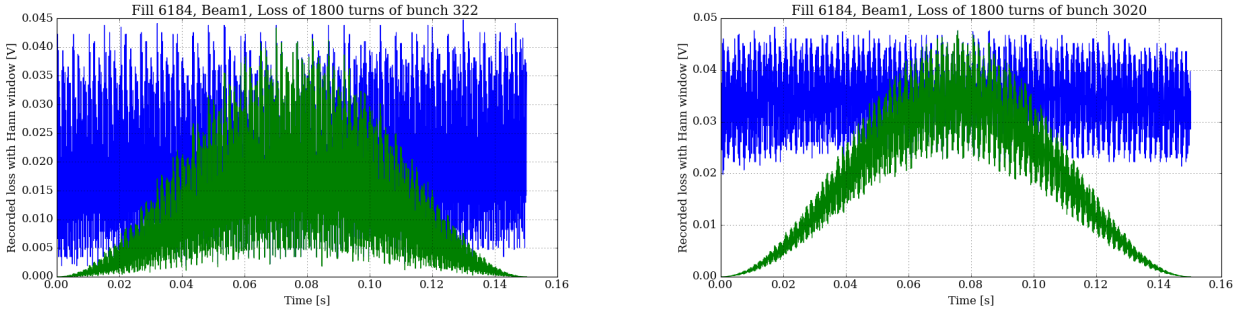

(a) **(b)**

Figure 27: The difference between the original signal (blue) and the one that is after applying Hann window (green). This pair represents one of bunches presented in Fig. 26

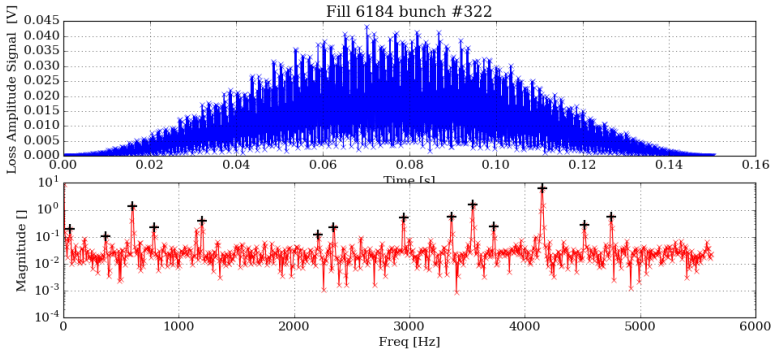

Figure 28: The effect of the FFT on the hanned signal.

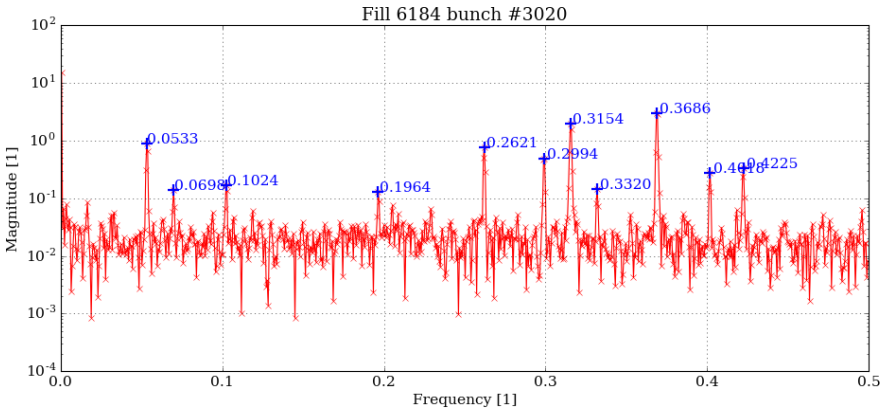

Figure 29: The FFT result here in equivalent sampling frequency (turn). Within many frequencies found, two are present in the region of the nominal betatron tunes $Q_x = 0.31$ and $Q_y = 0.32$.

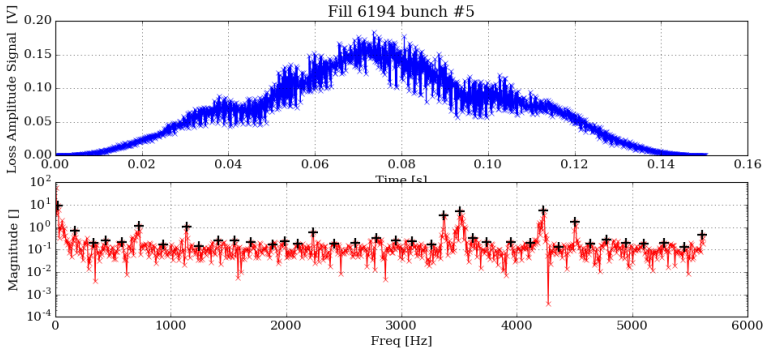

Figure 30: The effect of the the FFT on the hanned signal.

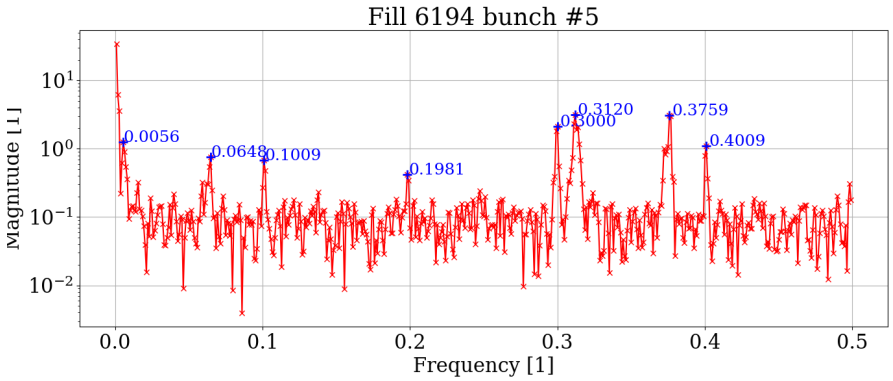

Figure 31: The FFT result here in equivalent sampling frequency (turn). Visible peaks around 0.3, two are present in the region of the nominal betatron tunes $Q_x = 0.31$ and $Q_y = 0.32$.

6 Summary and outlook

We presented some applications of the diamond BLM system installed in the LHC betatron collimation insertion. A selection of the results illustrates the potential of this measurement system to understand better the losses at the LHC. Measurements range from the bunch-by-bunch analysis in different phases of the operational cycle, to the frequency analysis of fast losses. This work will continue in 2018, in collaboration with the various teams at CERN. New hardware is planned to improve the system. The addition of one monitor per beam will allow distinguishing the horizontal and vertical contents of losses at primary collimators, thus opening the possibility for a better understanding of loss mechanisms and for further study of correlation with other bunch-by-bunch measurements.

For the 2018 we plan to put a first version of the loss analysis for the tune diagnostics for the CCC operators using for the time being the ROSY data format. In the mean time a CERN standardized VFC crate will be tested and validated in parallel in order to obtain the same functionality as now with ROSY boxes. We plan to move larger part of the logic into the FPGA unit in the VFC module and extract already bare bunch/train evolutions as showed e.g. in Sec. 2.2. Additionally we requested a second pair of diamond detectors, install after the horizontal collimator to disentangle losses from different planes.

Acknowledgements

Authors would like to thank to LHC OP crew that was eager to accept dedicated tests with the diamonds, as well as the BE–BI–BL team for some input on the hardware side. We would like to thank as well TE–MPE–PE members for a fruitful collaboration in the view of the diamonds installation in 16L2 and later with analysis of the data related to the 16L2 dumps.

References

[1] B. Salvant *et al.*, "Experimental Characterisation of a Fast Instability Linked to Losses in the 16L2 Cryogenic Half-Cell in the CERN LHC", presented at IPAC'18, Vancouver, Canada, Apr.-May 2018, this conference.

[2] C. Xu, "Using Diamond BLMs in the LHC", BI-Day 2017, 29th June 2017.

[3] S. Redaelli *et al.*, Installation in IR7 of Primary Crystal Collimators (TCPC) on Beam 2, LHC-TC-EC-0008, EDMS 1714148.

[4] Python to FESA/LSA/INCA interface via JAPC, `https://gitlab.cern.ch/scripting-tools/pyjapc`

[5] dBLMs EOS project space `/eos/project/dblm`, available from CERN computing infrastructure.

[6] CERN IT *et al.* `http://information-technology.web.cern.ch/services/eos-service`

[7] C. Xu, A. Gorzawski, `https://gitlab.cern.ch/dBLM_users`, *Only for CERN users*

[8] A.Gorzawski, `https://gitlab.cern.ch/agorzaws/dBLM-bbb-losses`

[9] B. Holzer, C. Zamantzas private communication

[10] A. Lasheen *et al.*, "Overview of the beams from the injectors", contribution at the LHC Operations Workshop in 2017, Evian, France, December 2017.

[11] *8th LHC Operations Evian Workshop*, Evian, December 2017

[12] A.Gorzawski *et al.*, "Bunch losses with diamond detectors", LBOC #82, 25 July 2017

[13] M. Solfaroli Camillocci *et al.*, "Combined Ramp and Squeeze to 6.5 TeV in the LHC", IPAC 16, Busan, Korea, 8 - 13 May 2016, pp.TUPMW031.

[14] A.Gorzawski *et al.*, "Luminosity Anti-leveling with Crossing Angle (MD 1669)", CERN-ACC-NOTE-2016-0058.

[15] M.Lamont, "Actions from Evian and Chamonix", LMC #296, 22 Mar 2017.

[16] M. Hostettler *et al.,* Beam size estimation from luminosity scans at the LHC during 2015 proton physics operation, Proc. of IPAC16, paper MOPMR025.

[17] J. Wretborn *et al.* "Study of off-momentum losses at the start of the ramp in the Large Hadron Collider ",Tech. Rep. CERN-ACC-NOTE-2017-0065 , CERN, Geneva

[18] G. Valentino, R. Bruce, A. Gorzawski, S. Redaelli, G. Trad, J. Wagner, C. Xu, "End-of-Fill Diffusion and Halo Population Measurements with Physics Beams at 6.5 TeV", Tech. Rep. LHC, June 2017 CERN, Geneva.

[19] A. Gorzawski, S. Redaelli, G. Valentino, J. Wagner, A. Mereghetti, "Beam diffusion mechanisms - EoF Halo Scraping MDs 2017", Tech. Rep. LHC , CERN, Geneva. (to be published)

[20] L.R. Carver *et al.*, "Instabilities and beam induced heating in 2016 (p. 141)", contribution at the LHC Operations Workshop in 2017, Evian, France, December 2017.

[21] B. Salvachua *et al.*, "Observation of the beam losses at the LHC during the reduction of the crossing angle." IPAC'17, TUPVA025

[22] `https://en.wikipedia.org/wiki/Hann_function`